# LARGE EDDY SIMULATION OF DROPLET STOKES NUMBER EFFECTS ON TURBULENT SPRAY SHAPE

***V. Vuorinen,[1,*] H. Hillamo,[1] O. Kaario,[1] M. Larmi,[1] & L. Fuchs[2]***

*[1]Aalto University School of Science and Technology, P.O. Box 14300, FIN-00076, Aalto, Finland*
*[2]Department of Mechanics, KTH, CICERO, SE-10044 Stockholm, Sweden*

[*]Address all correspondence to V. Vuorinen E-mail: ville.vuorinen@tkk.fi

*Original Manuscript Submitted: 8/13/2009; Final Draft Received: 1/11/2010*

*The spatial and temporal development of a spray strongly depends on the local characteristics of turbulence. The turbulence-droplet coupling gives rise to droplet dispersion, which is the underlaying physical phenomenon of interest in this study. Large eddy simulations (LES) provide details of the instantaneous flow field and anisotropy of the larger scales. Hence, LES has the potential of improved spray simulations in flows that are highly nonisotropic/nonstationary. A numerical study on the effect of droplet diameter (d) on spray shape is described by carefully varying d. The droplets are assumed to be non-interacting with each other. They are also assumed to maintain their shape and diameter. The droplet Stokes numbers are within the range* $0.07 \le \mathrm{St_p} \le 2.56$*, corresponding to diameters* $2 \le d \le 12\,\mu\mathrm{m}$ *for a common liquid fuel. In order to emulate a fuel spray, a droplet-laden jet at* $\mathrm{Re} = 10,000$ *and* $\mathrm{Ma} = 0.3$ *is considered as a model problem that avoids the dense spray regime. A novel technique to visualize the simulated sprays in a realistic manner is presented, and a qualitative comparison to a diesel spray experiments is made. It is shown that the spray-cloud shape depends strongly on droplet Stokes number. A spray penetration correlation formula is suggested. The nonlinear character of the droplet-eddy interaction and its dependence on droplet size is studied by visualization of droplet trajectories. We show that the spray behavior can be coherently explained by considering the statistical properties of the droplet cloud. The results show that the instantaneous/short-time-averaged probability density functions (PDFs) of droplet statistics explain very coherently the* $\mathrm{St_p}$ *dependency of the spray shape. The PDFs of the axial and radial components of droplet-gas slip velocity* $(\mathbf{u}_\mathrm{g} - \mathbf{u}_\mathrm{p})$ *are used to explain the visual observations on the spray cloud evolution.*

**KEY WORDS:** *large eddy simulation, Stokes number, fuel spray, droplet dispersion*

## 1. INTRODUCTION

The behavior of the combustion in a diesel engine strongly depends on the spray distribution prior to ignition. During the past decades, continuous efforts have been made to study alternative, more environmentally friendly diesel engine concepts. A highly interesting option is the homogeneous charge compression ignition (HCCI) engine in which the particulate and the NOx emissions could be substantially reduced (Akihama et al., 2001). Because the fuel injection in such an engine typically takes place at low temperature conditions, the spray evaporation during the injection is not the process-determining step as in a conventional diesel engine. Also, when far enough from an injector, the droplet breakup has become less important. Thus, in such a situation, the understanding of spray formation, including the transient spray penetration and the interplay between the fuel droplets and the turbulent gas, is highly relevant. The reason for this is that the momentum coupling between

 

## NOMENCLATURE

| | |
|---|---|
| $c$ | droplet to gas volume fraction |
| $d$ | particle/droplet diameter (m) |
| $p$ | pressure (N/m$^2$) |
| $u_i$ | $i$ component of velocity (m/s) |
| $C_D$ | particle drag coefficient |
| $D$ | diameter, inlet diameter of the PLJ in the model problem (m) |
| $\mathcal{M}$ | spray momentum source term |
| $\mathcal{P}$ | probability density function |
| Re | Reynolds number, Re $= U\delta/\nu$ |
| $S$ | spray penetration, RMS of droplet cloud $z$-coordinate (m) |
| $\mathrm{St_p}$ | Stokes number for a particle which primarily depends on $d^2$ |
| $T$ | integral time scale (s), temperature (K) |
| $U_o$ | inlet gas velocity (m/s) |
| $W$ | spray width, RMS of droplet cloud radial coordinate (m) |
| $\delta W_\mathrm{r}$ | radial slip velocity normalized with gas exit velocity ($\delta W_\mathrm{r} > 0$) |
| $\delta W_z$ | axial slip velocity normalized with gas exit velocity |
| **Greek Symbols** | |
| $\delta_{ij}$ | Kronecker symbol |
| $\varphi$ | mass loading ratio |
| $\nu$ | kinematic viscosity (m$^2$/s) |
| $\rho$ | density (kg/m$^3$) |
| $\tau_\mathrm{p}$ | particle momentum relaxation time (s) |
| $\tau_\mathrm{f}$ | integral time scale (s) |
| **Subscripts** | |
| c | characteristic |
| f | fuel/fluid |
| g | gas |
| inj | injection |
| p | particle/droplet |
| t | turbulent |

the droplets and the gas influences the premixing of (1) fuel droplets prior to the actual evaporation, and after that in the evaporation stage, (2) premixing of fuel vapor and in-cylinder gas. Hence, it is understandable that there has been a continuous interest within the diesel spray community to understand the spray processes better, not only in general, evaporative conditions (Heywood, 1989; Naber and Siebers, 1996), but also in nonevaporative conditions (Cao et al., 2000; Hillamo et al., 2008). Furthermore, because particle- and droplet-laden flows appear in several applications that often involve combustion, there has been a strong interest in the research community to understand the role of particle-turbulence interactions using both experimental and computational tools (Crowe et al., 1998; Elghobashi, 1994).

In general, the alternative modeling approaches for simulating the motion of a turbulent fluid can be divided into Reynolds-averaged Navier-Stokes (RANS), large-eddy simulation (LES), and direct numerical simulation (DNS) (Ferziger and Perić, 1999; Pope, 2001). RANS corresponds to the largest level of turbulence modeling in which all turbulent scales are modeled. One of the main issues with such an approach is that the larger scales are problem dependent and, hence, they do not lend themselves to general, problem-independent modeling. In contrast, in LES, only the smallest scales (i.e., those that are unresolved on the given grid) have to be modeled because the larger ones are resolved by the grid. If the grid is adequately fine, then the small-scale turbulence is, in general, isotropic and tends to be universal (i.e., problem independent) and, therefore, it can be more easily modeled. Once the resolution increases beyond the smallest scales of turbulence, LES becomes DNS (Pope, 2001). LES is becoming an increasingly popular approach due to its properties and because only reasonable computational power is required to solve many turbulent flow problems (Apte et al., 2009; Olsson and Fuchs, 1996).

During the past two to three decades, diesel spray simulations have been carried out, with RANS turbulence models which enable simulations on a single desktop computer on rather coarse grids with spatial and temporal resolution of order $\sim 10^{-3}$ m and $10^{-6}$ s, correspondingly. The main simulation method of the spray (droplet) phase is the Lagrangian particle tracking (LPT) method in which it is assumed that droplets obey a given equation of motion and that the droplets are pointlike momentum sources or sinks that interact with the carrier fluid with a characteristic particle momentum relaxation time scale $\tau_\mathrm{p}$. The LPT method, which neglects interparticle interaction, is therefore most suitable for the simulation of the dilute spray regime further downstream from the nozzle (Amsden et al., 1989; Kärrholm, 2008).

In the LPT spray modeling context, the family of KIVA codes include different submodels that are designed for handling sprays and combustion. The models have been tailored for the RANS framework (Amsden et al., 1989; Stiesch, 2003) and their purpose is to handle droplet breakup, droplet coalescence, and droplet dispersion. The latter model introduces the dispersion effects of turbulence (assuming local isotropy) on the droplets by adding a random velocity fluctuation to droplet motion (Amsden et al., 1989; Stiesch, 2003). The potential of improved modeling combined with the availability of computational power has made LES an attractive alternative, and recently a LES turbulence model has been implemented also to the KIVA codes. The experience showed that LES, unlike RANS, produces the desired, transient features of the flow field including random eddy structures (Hori et al., 2006). These differences imply that computational fluid dynamics (CFD) modeling of internal combustion (IC) engine processes is undergoing a paradigm change when going from RANS-based models to LES-based models. From the viewpoint of this work, one of our missions is to show that, in LES, droplet dispersion can be produced without a dispersion model because, in LES, the turbulent length and time scales of the energy-containing eddies are directly available, which implies that in certain situations one does need to model the weak subgrid-scale effects (e.g., the dispersive effect of turbulence with adequate grid resolution).

In sprays that contain huge numbers of droplets, computing the trajectory of each droplet may require a too long computational time and, hence, one tracks groups of droplets that have similar properties. This approach is the so-called parcel method, in which the motion of $N$ parcels is tracked (Amsden et al., 1989). Each of the parcels contains a given number of physical particles/droplets that all have same properties (e.g., diameter, mass, temperature, etc.). As the computational grid is refined, the number of parcels has to increase (Stiesch, 2003), which implies that the number of droplets in each parcel decreases. There is inherently a problem with very fine grids because a basic assumption of Lagrangian particle tracking (LPT) is that the droplets (and parcels) are nondisplacing, which requires that the volume of a droplet (or the total volume of droplets in a parcel) is much smaller than that of the cell volume. However, computational time demands limiting $N$ typically to rather small values (e.g., $N = 350,000$ in this work).

Apparently, LPT is associated with conceptual and computational difficulties as the computational grid spacing decreases. Engine modelers have also noted that the type of the computational grid may have a major impact on the shape of the spray cloud (Stiesch, 2003). From the viewpoint of numerical stability, problems appear when several conditions are met simultaneously: (1) the particle mass approaches the mass of the carrier fluid within a given computational cell, (2) when the particle time, $\tau_{\rm p}$, is small, and (3) when the relative velocity [i.e., droplet-gas slip velocity $(\mathbf{u}_{\rm g} - \mathbf{u}_{\rm p})$] is large. Under such conditions, the local flow behavior is incompatible with the underlying assumptions of LPT modeling. However, high-fidelity LES studies have been performed by several groups also in the context of sprays using LPT schemes and it can be stated that, if correctly applied, LES and LPT can reproduce experimentally observed mean and fluctuating spray characteristics (Apte et al., 2003a,b, 2009; Oefelein et al., 2007). Nevertheless, due to the mentioned difficulties of LPT, it is understandable that many of the previous LES and DNS studies on particle-laden flows have been limited to rather low particle loadings (Ling et al., 1998; Vuorinen et al., 2007, 2008; Yan et al., 2008).

In this work, we focus our attention to spray formation processes and study the mixing of droplets in a turbulent gas. Because the problem is clearly highly transient, LES is chosen to simulate the motions of the turbulent carrier phase and LPT is used to handle the equations of motion of the droplets. As explained above, the assumptions of LPT become incompatible when the grid spacing becomes too small. Hence, we simulate the dilute spray regime in a model problem of particle-laden jet (PLJ)/droplet-laden jet that emulates a fuel spray far from an injector and avoids the ”singular” near-nozzle regime. The PLJ forms the base flow in which an initially laminar momentum stream of gas erupts into a chamber, the gaseous flow undergoes transition into turbulence due to high shear via growth of the Kelvin-Helmholtz (KH) instability, and hence, the eventually turbulent jet provides an environment in which droplet dispersion can be efficiently studied (Borman and Ragland, 1998; Grinstein et al., 2007).

From previous studies on particle dispersion in free shear flows, it is expected that the development of the spray can be characterized as a function of droplet diameter $d$ (see Section 3.2 for further discussion). The effects of droplet diameter enter in the form of the time it takes for the droplet to adjust to the local flow conditions. This time, $\tau_{\rm p}$, is related to the time scale of the flow, $\tau_f$, which results in the Stokes number $\mathrm{St_p} = \tau_p/\tau_f$ ($\mathrm{St_p} \propto d^2$). The paper aims at statistical characterization and visualization of droplet size effects in mono- and polydisperse particle-laden round jets. The paper enriches the picture of two-way momentum coupling and the temporal aspects of the spray problem. The relation between small- and large-scale behavior of the spray are explained: the spray shape dependence on $\mathrm{St_p}$ is explained by computing the probability density functions (PDFs) of radial and axial components of particle-gas slip velocities ($\mathbf{u}_g - \mathbf{u}_p$) over the whole droplet cloud. An important achievement of the paper is that, although the problem itself is of transient character, the considered (short-time-averaged/instantaneous) PDFs provide a very coherent way of distinguishing between different sprays and explaining visual spray observations. We are not aware of a more detailed and systematic study of two-way coupling for particle-laden jets in the low $\mathrm{St_p}$ regime.

## 2. NUMERICAL MODELING

### 2.1. Computational Setup and Boundary Conditions

The computational setup, depicted in Figs. 1 and 2, consists of a cylindrical chamber into which a round gaseous jet is injected. The diameter of the chamber is $8D$, and its length is $35D$. At the walls, isothermal temperature and no-slip velocity boundary conditions are used; whereas at the inlet, temperature and velocity are specified. At the outlet, the pressure is fixed to a constant value and the zero-gradient condition is used for the velocity if fluid flows out of the domain. The jet diameter is $D = 2$ mm and the gaseous stream enters into a cylindrical chamber through an inlet with mean velocity $U_o = 80$ m/s. The inlet velocity profile is a top-hat profile with mean velocity $U_o$ that is perturbed with uniformly distributed random noise and the amplitude of the fluctuating component is $0.05U_o$. This corresponds to an average gas flow rate of $\dot{m}_g = 1.54 \times 10^{-3}$ kg/s through the inlet.

Droplets are introduced into the jet randomly at the inlet, and the velocity of the droplets is $1.25U_o = 100$ m/s. The flow rate of the droplets is $\dot{m}_p = 0.3\dot{m}_g$; thus, the mass loading ratio is $0.3$. The density of the droplets is $\rho_p = 830$ kg/m$^3$, and due to the low Mach number (Ma = 0.3), the density of the gas is approximately a constant $\rho_g \approx 6.0$ kg/m$^3$, resulting in the density ratio $\rho_g/\rho_p \approx 0.0073$. The Reynolds number of the gaseous jet is Re $= U_o D/\nu_g = 10^4$, which is a typical order of magnitude in spray applications. The kinematic viscosity of the gas is approximately $\nu_g \approx 1.6 \times 10^{-5}$ m$^2$/s. The non-dimensional total injection time is $\tau_{inj} = 60T = 1.5$ ms, where the integral timescale is defined by $T = D/U_o$. The computational domain chosen here is such that the boundaries do not affect the development of the jet and the spray. In the simulations pre-

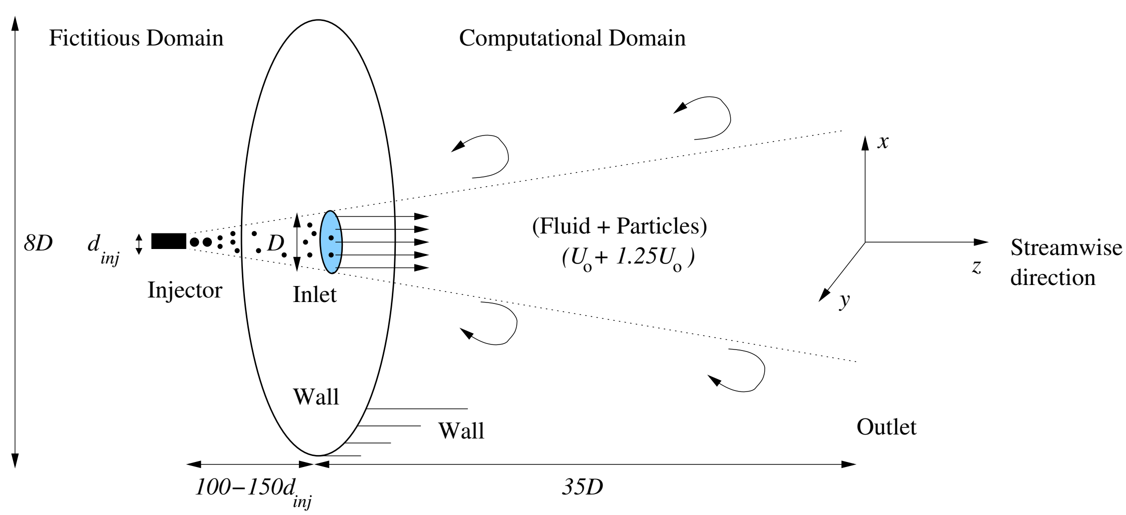


**FIG. 1:** Flow configuration, inflow and outflow boundary condition: droplets are injected uniformly from the inlet area into the gaseous jet. The mean gas jet velocity at inlet is $U_o = 100$ m/s and the initial droplet velocity is $1.25U_o$. The diameter and the length of the chamber are $8D$ and $35D$, correspondingly ($D = 2$ mm). The current setup avoids solving a dense near-nozzle region by modeling the spray as a particle-laden jet.

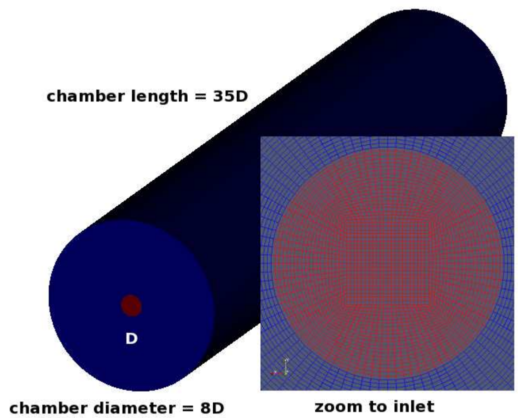


**FIG. 2:** Computational domain and zoom to the inlet of the mesh. The present mesh is composed of blocks, which is important because this avoids the singularity in the origin that is associated with, e.g., a polar mesh.

sented herein, the droplets do not reach beyond a distance of $z = 20 - 25D$.

The characteristic properties of gas jets and their numerical simulation have been described in the literature (Borman and Ragland, 1998; Hällqvist, 2006; Olsson and Fuchs, 1996). The base flow consists of a growing shear layer along the outer portion of the jet and the potential core region, which extends to $4 - 5D$ from the inlet until the shear layer merges. This core region is the ”most laminar” region of the spray, and its length is usually characterized by constant mean axial velocity ($U = U_o$) along the $z$-axis (Olsson and Fuchs, 1996; Vuorinen et al., 2007, 2008). The potential core is considered to end when the axial velocity starts to decay after $4 - 5D$ from the inlet. After the potential core, a transitional region begins that is approximately $10D$ long, after which the flow becomes fully developed (Borman and Ragland, 1998; Olsson and Fuchs, 1996). The shear layer instability is of the Kelvin-Helmholtz (KH) type and, in single-phase jets, considered to be the mechanism for the growth of shear layer vortices, vortex roll up, and merging which eventually leads to transition into turbulence (Grinstein et al., 2007; Olsson and Fuchs, 1996). One way to see this is shown in Fig. 3, which considers the spectra of radial velocity components for the different simulation cases at two different positions along the shear layer of the jet. In single-phase jets, the KH instability manifests itself as peaks in the spectra near the inlet due to vortex shedding (Hällqvist, 2006; Olsson and Fuchs, 1996). Furthermore, it is seen that, at the end of the potential core ($z/D = 4.5$), the peaks have disappeared due to vortex pairing and the flow has become turbulent. As a result, it can be deduced that a range of frequencies are resolved by the numerical algorithm.

Figure 2 shows the computational domain and a zoom to the inlet. The mesh is composed of nine blocks that fill the cylinder. The jet enters into a region composed of five blocks, including a Cartesian grid in the center. This construction allows better numerical accuracy and also avoids the singularity of polar meshes at the $z$-axis.

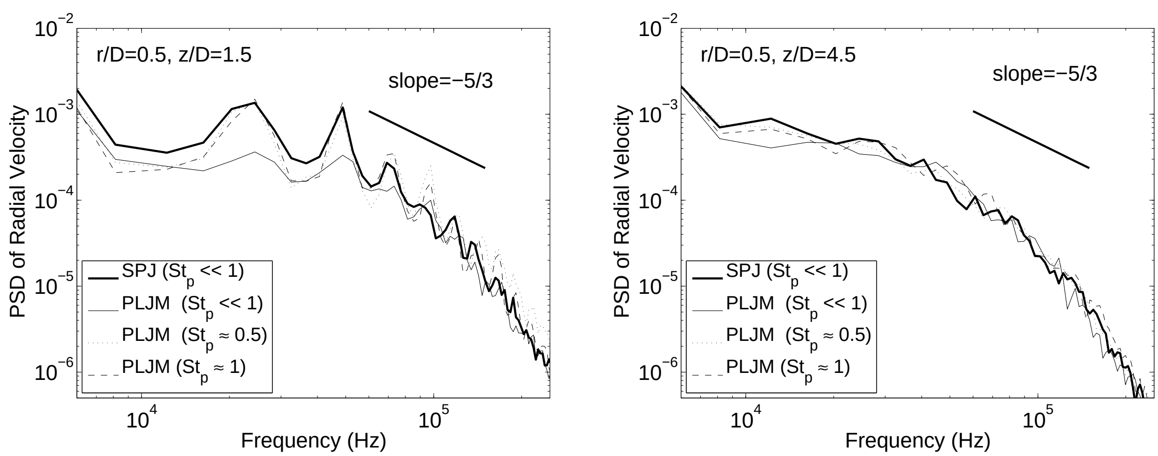


**FIG. 3:** Spectra of radial velocity components along the shear layer. Left: from $z/D = 1.5$. Right: from $z/D = 4.5$. It is seen that (1) the Kelvin-Helmholz instability manifests itself as characteristic peaks near the inlet and the peaks are damped for the smallest droplets, (2) further downstream the peaks have disappeared due to vortex merging, and (3) a range of time scales is being resolved.

The grid resolution depends on the streamwise direction in such a way that the grid spacing increases gradually in the downstream direction. The ratio between the "thickest" and the "thinnest" cell layer is 3 so that the mesh is very fine in the streamwise direction near the inlet and gradually becomes coarser. The mesh contains about 3.5 million cells. The number of cells in streamwise direction is 300, whereas 110 cells are used to cover the space between the edge of the inlet and the sidewall. It has been noted that even with a coarser mesh, used in a previous study, the algorithm captured a range of scales providing a scale separation between the large scales of turbulence and the smallest resolved ones (see Vuorinen et al., 2007). This is important for demonstration of droplet Stokes number effects on spray dynamics because the effect of a range of frequencies can be captured by the mesh resolution, as seen from Fig. 3. In comparison to Vuorinen et al. (2007; 2008), the present mesh is made even finer from the inlet region and the jet shear layer. The smallest cells in the mesh are located in the jet axis and about $D/60 \times D/60 \times D/20$ in size. It is estimated that, in the present simulations within the spray region, the mesh resolution in the $z$ direction is always smaller than $D/10$ and in the radial direction smaller than $D/20$. Hence, in view of estimates of the Taylor microscale for jets at Re $\sim 10^4$ by Olsson and Fuchs (1996), the present resolution is adequate as implied also in Fig. 3.

## 2.2. Governing Equations and Numerical Algorithms

### *2.2.1. Fluid Motion*

The governing equations for the gaseous phase, describing the conservation of mass, momentum, and energy are as follows:

$$\frac{\partial \rho}{\partial t} + \frac{\partial \rho u_j}{\partial x_j} = 0 \tag{1}$$

$$\frac{\partial \rho u_i}{\partial t} + \frac{\partial (\rho u_i u_j)}{\partial x_j} = -\frac{\partial}{\partial x_j}(-p\delta_{ij} + \sigma_{ij}) + \mathcal{M} \tag{2}$$

$$\frac{\partial \rho e}{\partial t} + \frac{\partial (\rho u_j h)}{\partial x_j} = \frac{\partial}{\partial x_j}(\sigma_{ij} u_i) + \frac{\partial}{\partial x_j}\left(\lambda \frac{\partial T}{\partial x_j}\right) \tag{3}$$

where $\mathcal{M} = \mathcal{M}(x, y, z, t)$ represents momentum sources in the momentum equation due to the force that the droplets exert on the carrier phase. The viscous stress tensor is defined as

$$\sigma_{ij} = \mu\Big(\frac{\partial u_i}{\partial x_j} + \frac{\partial u_j}{\partial x_i}\Big) - \mu\frac{2}{3}\frac{\partial u_i}{\partial x_i}\delta_{ij} \tag{4}$$

In LES, the Eqs. (1)–(4) are spatially filtered assuming that the filtering operator is commutative with the differential operator (Pope, 2001). The filtering of the linear terms leads to the same terms for the filtered variables. In contrast, the filtering of the nonlinear terms leads to a similar term with the filtered variables with additional subgrid-scale (SGS) terms. These terms cannot be expressed in terms of the filtered variables due to the nonlinearity of the governing equations (Grinstein et al., 2005; Pope, 2001). When the resolution of the simulation is fine enough (i.e., capturing very large portion of the kinetic energy of the turbulent fluctuations), the SGS terms have only minor contribution and, therefore, they can be neglected altogether since the role of the SGS terms is to account for the interaction between the resolved and the unresolved scales. Dissipation of turbulent energy takes place at the smallest (Kolmogorov) scales (Grinstein et al., 2007; Pope, 2001). Thus, the role of the SGS term has to be accounted for explicitly (e.g., by an explicit SGS model) or implicitly (e.g., through a numerical scheme).

In this work, the turbulence of the gaseous phase is simulated using the LES approach. The governing equations are discretized on a hexahedral grid, as seen in Fig. 2. The convective and viscous terms are both discretized using second-order accurate centered schemes. The time derivatives are discretized using a second order accurate implicit scheme. The solver uses the pressure implicit with splitting of operator (PISO) method for solving the pressure correction (Ferziger and Perić, 1999). Details on the implementation and validation of the numerical schemes of the present code are provided in (Berglund, 2006; OpenCFD, 2010; Jasak, 1996). Equations (1)–(4) are numerically solved for the filtered variables, and the SGS terms are neglected. In our calculations, the resolution and the numerical dissipation have been found to be adequate to resolve a range of frequencies so that the large-scale motions are adequately captured (Vuorinen et al., 2007). This is called the *implicit* LES approach (Grinstein et al., 2005, 2007; Salewski and Fuchs, 2007; Vuorinen et al., 2007) and because no explicit SGS-model is employed, the viscous stress tensor Eq. (4) includes only the molecular effects and thus no contribution from a turbulent viscosity as explicit SGS-models. Furthermore, the dynamic viscosity of the gas is almost a constant due to small variation of density.

*2.2.2. Droplet Motion*

In LPT, one has to track the motion of individual droplets. In a diesel spray, the number of droplets is very large and, hence, LPT may become computationally heavy. Because the motion of the droplets is not independent of each other, one may group neighboring droplets with similar properties into a "parcel". Each parcel is then tracked as if it was a single droplet having the (averaged) properties of the droplets in the parcel. In the implementation of the present simulation code, every parcel contains the same amount of mass and a certain number of droplets that all have the same shape (spherical) and the same diameter. Furthermore, it is assumed that the droplets do not evaporate nor break and there is no direct interaction between the drops.

The motion of the droplet parcels is governed by Newton's equation of motion (Amsden et al., 1989; Borman and Ragland, 1998; Heywood, 1989). It is assumed that the force acting on a droplet is due to the drag (with the coefficient $C_D$). The droplet (i.e., parcel) equation of motion reads

$$\frac{1}{6}\rho_{\mathrm{p}}\pi d^3 \frac{d\mathbf{u}_{\mathrm{p}}}{dt} = \frac{1}{2}(\mathbf{u}_{\mathrm{g}} - \mathbf{u}_{\mathrm{p}})|\mathbf{u}_{\mathrm{g}} - \mathbf{u}_{\mathrm{p}}|\rho_{\mathrm{g}} C_D \frac{\pi d^2}{4} \quad (5)$$

Equation (5) can be cast into the following form

$$\frac{d\mathbf{u}_{\mathrm{p}}}{dt} = \frac{C_D}{\tau_{\mathrm{p}}}\frac{\mathrm{Re}_{\mathrm{p}}}{24}(\mathbf{u}_{\mathrm{g}} - \mathbf{u}_{\mathrm{p}}) \quad (6)$$

which is useful due to the explicit appearance of the droplet time scale defined as

$$\tau_{\mathrm{p}} = \frac{\rho_{\mathrm{p}} d^2}{18\rho_{\mathrm{g}}\nu_{\mathrm{g}}} \quad (7)$$

The droplet Reynolds number is defined by

$$Re_{\mathrm{p}} = \frac{|\mathbf{u}_{\mathrm{g}} - \mathbf{u}_{\mathrm{p}}|d}{\nu_{\mathrm{g}}} \quad (8)$$

and the expression for the drag coefficient $C_D$ is given by

$$C_D = \begin{cases} \dfrac{24}{\mathrm{Re}_{\mathrm{p}}}\left(1 + \dfrac{1}{6}\mathrm{Re}_{\mathrm{p}}^{2/3}\right) & \mathrm{Re}_{\mathrm{p}} < 1000 \\ 0.424 & \mathrm{Re}_{\mathrm{p}} \geq 1000 \end{cases} \quad (9)$$

The parcel position is updated through

$$\frac{d\mathbf{x}_{\mathrm{p}}}{dt} = \mathbf{u}_{\mathrm{p}} \quad (10)$$

The parcels are advanced in time using a semi-implicit time integration method by taking five subiterations within each time step. The instantaneous momentum source $\mathcal{M}(x, y, z, t)$ is evaluated for each cell separately by looping over all the parcels in a given cell, computing the lost momentum during the time step by computing the velocity change from Eq. (6), and multiplying the acceleration by the parcel mass. During a time step, it is also possible that a parcel moves from one cell to another. If this is the case, then the released/absorbed momentum is computed and shared between the cells accordingly (proportional to the time fraction the parcel spends in the associated cells inside the time step). More details on the implementation of the LPT schemes and submodels in the present code are described in Kärrholm (2008), Kärrholm and Nordin (2008), and OpenCFD Ltd. (2010).

As noted in Eq. (6), an important nondimensional number (i.e., the Stokes number) may be defined as

$$\mathrm{St}_{\mathrm{p}} = \tau_{\mathrm{p}}\frac{U_o}{D} \quad (11)$$

Here, $\mathrm{St}_{\mathrm{p}}$ is referred to the mean flow time scale $T = \tau_{\mathrm{f}} = D/U_o$, which is a good measure in the proximal region of the jet because the energy-containing frequencies in this region are of the order $f \sim 1/T$. In general, it should be noted that Eq. (5) is quadratic in terms of the slip velocity (and also in $d^2$). This makes the coupling between the droplets and the gaseous phase nonlinear.

It should be noted that one of the features involved with present LES + LPT is that the grid cannot be made much finer because this would be inconsistent with the assumption that the droplets do not displace the carrier fluid. Another issue associated with LES is the time-step size. With improved spatial resolution, smaller time steps must be used. The minimum droplet relaxation time, $\tau_{\mathrm{p}}$, sets a restriction to the time-step length $\Delta t$ in the droplet equations, which should be smaller than the smallest droplet momentum relaxation time. In the simulations, $\Delta t \ll \min(\tau_{\mathrm{p}})$ so that the droplet motion becomes resolved also for the smallest droplets. The inverse of $\tau_{\mathrm{p}}$ is proportional to the change in the force that the droplet motion has on the carrier phase. Thus, very small values of $\tau_{\mathrm{p}}$ lead to a large change in the right-hand side of the momentum equations, which may lead to numerical instability. For the large droplets having a large $\mathrm{St}_{\mathrm{p}}$, the numerical stability problems are small because the cell-droplet momentum interaction is small as compared to the other terms in the momentum equations.

As pointed out above, good resolution LES implies that the subgrid-scale fluctuations are weak and hence can hardly modulate droplet motion. If this is not the case, then one may add the effects of the SGS fluctuation in a way similar to the one used in the RANS framework. Thus, from the SGS model, one may assess the magnitude of the SGS velocity fluctuation. Then, a random vector of length equal to the local SGS speed can be generated and is added to the resolved velocity when computing the acceleration of the droplet. Apte et al. (2003a), have pointed out two aspects regarding the effect of subgrid scales on the particles: (1) the effect of subgrid scales modeling is assumed to be important when there is a large amount of kinetic energy in the subgrid scales and when the SGS time scale is large in comparison to the characteristic droplet timescale, and (2) if a SGS model is employed, then the particles do feel the effect of the subgrid scales by the resolved scale velocities. However, an example of a LES where the effect of SGS fluctuations on the droplet motion is explicitly considered was carried out by Oefelein et al. (2007). The authors considered the effect of subgrid scales on droplets by assuming the SGS velocity fluctuation to originate from a stochastic *Wiener process* (Pope, 2001). Probably, in that particular case, it is consistent to consider the effect of SGS fluctuations on the droplets because an explicit SGS model for $k$ is used. In this study, however, it is assumed that the effect of subgrid scales on the particle motion is small and, hence, Eqs. (5)–(10) are used as such to simulate the droplet motion.

### 2.3. The Computational Cases

The main parameter that is studied is droplet diameter ($d$). Hence, the main results are related to nine simulations of monodisperse sprays in which $d$ is varied between $2$ and $12$ μm. Because $\mathrm{St_p}$ depends directly on $d^2$, this corresponds to the range $\mathrm{St_p} = 0.07 - 2.56$. This range is of interest due to time-scale interaction between droplets and the gaseous phase because $\mathrm{St_p} \gg 1$ would yield trivial dynamics (ballistic trajectories) and $\mathrm{St_p} \ll 0.1$ would not be temporally resolved. Hence, interesting differences in mixing are expected to be seen within this range. We also carried out three simulations of polydisperse sprays having a uniform parcel size distribution. This translates to a $\mathcal{P}(d) \sim d^{-3}$ probability distribution in terms of droplet sizes because all the computational parcels have the same mass. In the polydisperse sprays, the parcel diameters are randomly chosen from a uniform distribution so that $\mathrm{St_p} = 0.07 - \mathrm{St_{p,max}}$, where $\mathrm{St_{p,max}}$ is given the values $\mathrm{St_{p,max}} = 0.7, 2.56$, and $5.1$. This is done in order to see how the average size of the distribution changes the spray character. The mono- and polydisperse simulations were carried out with the mass loading of $\varphi = 0.3$. For comparison between one- and two-way coupled jets, we also carried out one simulation of a single-phase gaseous jet with a negligible amount of tracer particles having $\mathrm{St_p} = 0.07$. In Section 3, the particle-laden monodisperse spray simulations are referred to as PLJM and the corresponding polydisperse simulations are referred to as PLJP. The single-phase jet simulation is referred to as single phase jet (SPJ).

## 3. RESULTS

### 3.1. LES versus Spray Visualization

We have noted that, although it is very instructive to visualize the simulated sprays by simply plotting the parcels, this approach yields a rather unrealistic picture in comparison to spray photographs (Ling et al., 1998; Vuorinen et al., 2007, 2008; Yan et al., 2008). Hence, it is desirable to visualize the sprays in a more realistic way. A simple but novel visualization algorithm can be implemented as follows. First, the light-of-sight spray mass intensity is calculated on a rectangular grid of 150 by 400 pixels using the droplet coordinates [say, using the $(x, z)$ pair]. The result is then convoluted with a Gaussian filter (with filter width of order one pixel), which make the image look somewhat smoother. Finally, the resulting pixel intensity (parcels/pixel) is damped with an exponential function to attain a realistic luminosity. The damping constant can then be chosen to be of the same order as the average pixel mass intensity within the spray region (e.g., 15 parcels/pixel) so that the contrasts are well seen. This algorithm can be used to better understand the relation between the current results and experimental diesel sprays, including the transient features of the model. In contrast to a spray, the PLJ does not start from a "point" injector. Hence, the comparison is done by simply moving the PLJ images on top of an experimental spray photograph so that the initial part of the spray is taken from shadowgraph images and the rest (most) of the spray is taken from the LES results.

Figure 4 shows how droplet size affects spray shape at various stages during injection. At early times, the largest droplets show a characteristic mushroom-shaped cloud, which results from droplet interactions with a tip vortex (Vuorinen et al., 2007). It is also seen that ini-

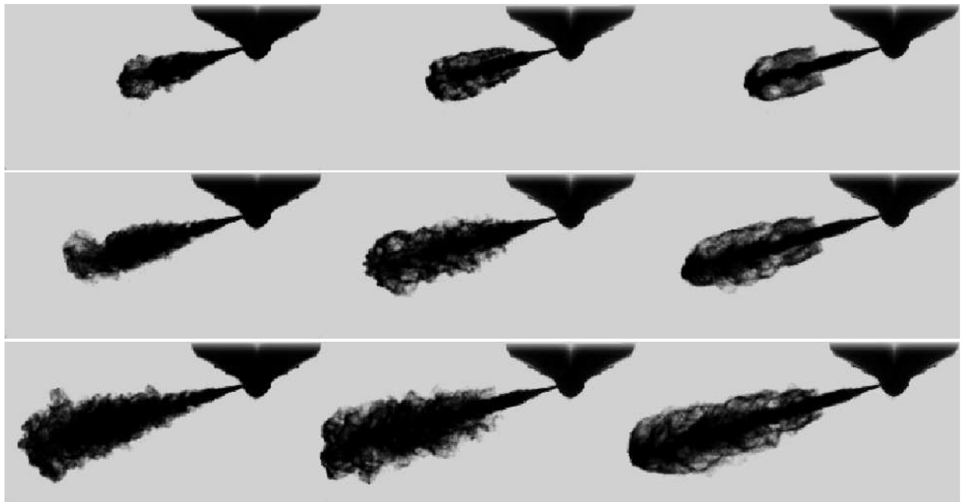

**FIG. 4:** Demonstration of droplet cloud evolution at three different times in the model problem. The initial part of the spray is not simulated. The boundary condition for the PLJ is given as shown in Fig. 1. Column 1: $\mathrm{St_p} = 0.07$. Column 2: $\mathrm{St_p} = 0.44$. Column 3: $\mathrm{St_p} = 2.56$. The difference in cloud shapes between small and large droplets is seen.

tially the large droplets only propagate to the injection direction along the spray axis because the spray angle is not modeled. In contrast, although the spray angle is not modeled, the small droplets that start to disperse in a more effective way starting from the inlet due to the shear layer vorticity that is able to centrifuge the droplets and hence a spray angle is formed. From Fig. 3, it can be deduced that the small droplets interact with the small shear-layer vortices, which is seen as dampening of the characteristic peaks. For the largest droplets, no interaction with the small scales occurs and, hence, the characteristic peaks, as observed in single-phase jets, are clearly observable (Hällqvist, 2006; Olsson and Fuchs, 1996). At late times, the sprays have evolved into quasi-stationary clouds the shape of which is seen to depend quite strongly on droplet size as will be further analyzed later. Finally, a comparison between LES and shadowgraph images of diesel sprays in Fig. 5 shows that, although the LES and the shadowgraph images are different in many ways, the general shape of the sprays is well reproduced by LES. For example, LES is seen to reproduce the transient and irregular shape of the spray boundary. Encouraged by the apparent realism of the new visualization technique and the similarity between the shadowgraph and LES sprays, we consider the effects of droplet size on the spray shape in more detail in Section 3.2.

### 3.2. Effect of Droplet Size on Spray Shape

The present results compare qualitatively well to several previously reported studies. Numerical studies (using DNS/LES) on the effect of $\mathrm{St_p}$ on particle dispersion in particle-laden plane jets and mixing layers in the one-way coupling regime by Ling et al. (1998), Luo et al. (2006), Yan et al. (2008) and others (cf. Apte et al., 2003a,b, 2009; Lieuwen and Yang, 2005; Oefelein et al., 2007) compare favorably to the present results. For example Ling et al. (1998) noted that particles with $\mathrm{St_p} \ll 1$ may be homogeneously distributed in a temporal mixing layer, but particles with $\mathrm{St_p} \sim 1$ may be preferentially concentrated on the periphery of eddies. Similar result was reported by Menon (2005). An example on particle dispersion, being quite similar to the present study, is related to a particle-laden plane jet as studied by Yan et al. (2008) at Re = 3000 with one-way coupling. The authors noted that the particles with $\mathrm{St_p} = 0.01$ and $0.1$ were well dispersed by the jet. At $\mathrm{St_p} = 1$, it was noted that the particles were more localized and also interacted visibly with the large-scale motions in the jet. At $\mathrm{St_p} = 10$, the particles were able to exit from the jet region only through the tip of the jet, and at $\mathrm{St_p} = 100$, the particles did not interact visibly with the turbulence due to their extremely slow response time to the flow time scales. Furthermore, the authors noted that, at $\mathrm{St_p} = 10$,

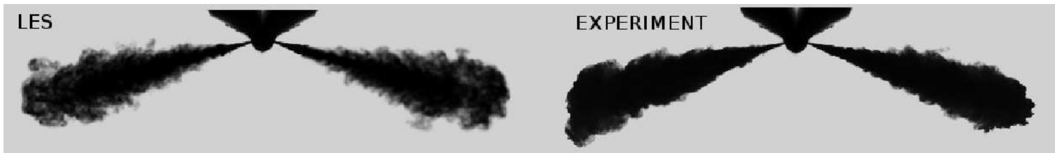


**FIG. 5:** Qualitative comparison on the spray shapes as obtained with LES (left) and shadowgraphy (right). In the LES image, the initial part of the spray has not been simulated but rather taken from the shadowgraphy images on the right. The boundary condition for the PLJ is given as shown in Fig. 1.

the dispersion was enhanced further downstream especially for $t > 30T$. However, in contrast to the previous studies with one-way coupling, the current study is carried out using a two-way coupling.

A feature characteristic to sprays is that during the injection the spray is highly nonstationary. As the tip of the spray penetrates into the gaseous environment, it gives rise to strong spatial and temporal induced flow in the carrier fluid. In the present studies, the spray extends up to distances of about $z/D = 20$ over simulation time of $\tau_{\mathrm{inj}} = 60D/U_o$. Thus, at least the first half of each simulation is highly nonstationary everywhere in the spray region. The flow of the gaseous phase undergoes transition into turbulence. However, after the transition period at times $t > 30T$, the spray clouds have developed into a quasi-stationary state with properties comparable to single-phase jets. Figures 6–8 show the light-of-sight images of some different cases. Figure 6a shows differences between SPJ and, in Fig. 6b–6d PLJM. In the SPJ case, the shear layer vortices and the growth of the Kelvin-Helmholtz-instability are visualized very clearly by tracer particles having $\mathrm{St_p} = 0.07$. These vortices are observed along the shear layer of the jet especially well when $z/D < 4$ in Fig. 6a. In line with the literature and previous studies (Borman and Ragland, 1998; Ferrand et al., 2003; Olsson and Fuchs, 1996; Vuorinen et al., 2007, 2008), the potential core of the SPJ ends at $z/D \approx 4$ after which the flow becomes turbulent and the axial velocity of the jet starts to decay (Olsson and Fuchs, 1996; Vuorinen et al., 2007, 2008). Interaction of the tracers with the shear-layer vortices can be clearly seen during the whole simulation. The spreading pattern is analogous to the passive scalar problem, because the tracers have a small $\mathrm{St_p}$ and their total mass is very small (i.e., one-way coupling). The situation for PLJ is similar, but now there is a two-way coupling between the droplets and the shear-layer vortices. The effect of increased mass loading is to increase the length of the potential core and to make the spray penetrate further downstream, increasing the spray volume (Vuorinen et al., 2008). However, as the mass loading here is only $\varphi = 0.3$, the length of the potential core of the PLJ is also about $4 - 5D$ (Ferrand et al., 2003; Vuorinen et al., 2007, 2008). In general, the small droplets form a foglike cloud that can be seen especially clearly when $\mathrm{St_p} < 0.4$. Here, the spray "looks" random already at the length scale to which $\mathrm{St_p}$ is referred. Because, in the present case, the inlet boundary

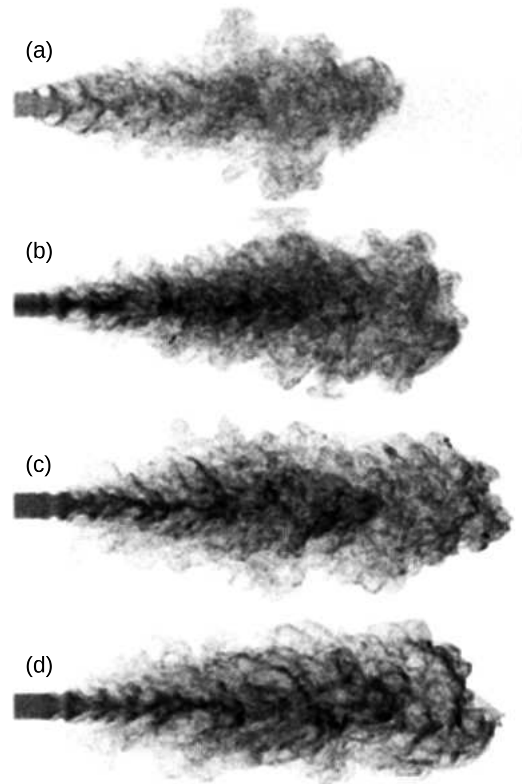


**FIG. 6:** Spray visualization. The contrast difference is created by exponentially damping the pixel mass intensity to achieve realistic luminosity. (a) SPJ ($\mathrm{St_p} = 0.07$), (b) PLJM ($\mathrm{St_p} = 0.07$), (c) PLJM ($\mathrm{St_p} = 0.28$), and (d) PLJM ($\mathrm{St_p} = 0.44$).

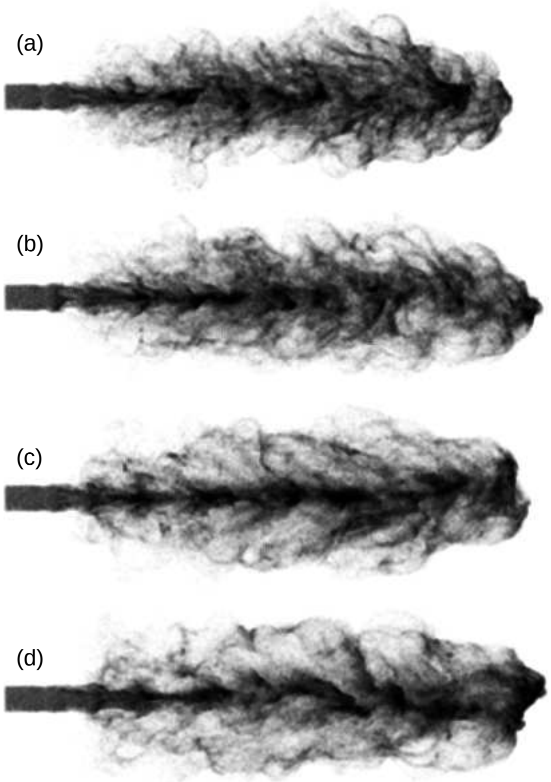


**FIG. 7:** Spray visualization. (a) PLJM ($\mathrm{St_p} = 0.64$), (b) PLJM ($\mathrm{St_p} = 1.14$), (c) PLJM ($\mathrm{St_p} = 1.78$), and (d) PLJM ($St_\mathrm{p} = 2.56$).

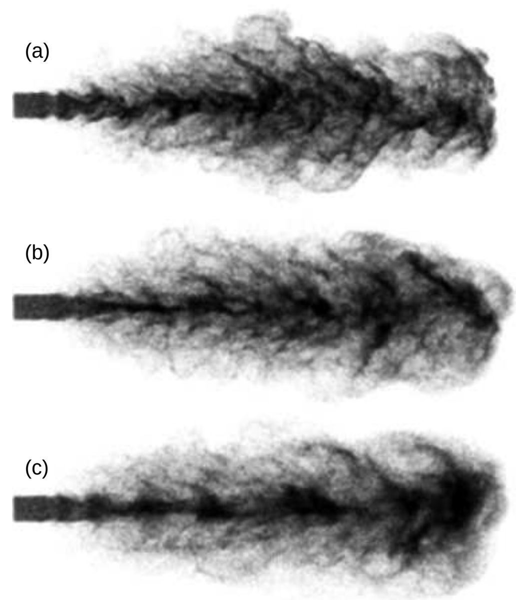


**FIG. 8:** Spray visualization. (a) PLJP (average $\mathrm{St_p} = 0.31$), (b) PLJP (average $\mathrm{St_p} = 1.23$), and (c) PLJP (average $\mathrm{St_p} = 2.26$).

condition is a laminar velocity profile, the potential core region is also partly laminar and, thus, the turbulence can be best seen to start along the shear layer and especially after the end of the core when $z/D > 4$.

Clear changes in the cloud shape can be seen when $\mathrm{St_p}$ exceeds the value of $\mathrm{St_p} = 0.5$. As $\mathrm{St_p}$ increases even more and eventually approaches the terminal value of 2.56, the concentration of droplets along the centerline becomes more and more pronounced (see Fig. 7 and also Fig. 8). Large $\mathrm{St_p}$ implies that the droplets will initially mostly propagate only to the streamwise direction because the shear layer vorticity is small and the large droplets are weakly affected by the small vortices. This effect is further enhanced because the flow is not fully turbulent within the potential core region. At later times, after the end of the potential core, the large droplets meet large eddies and their dispersion away from the centerline is enhanced. The simulation results herein are qualitatively, for different $\mathrm{St_p}$, very much in line with many previous studies, although the applications and setups are somewhat different (c.f. for example Apte et al., 2003a,b, 2009; Oefelein et al., 2007).

### 3.3. Spray Penetration and Width

In order to understand how the spray cloud develops on average, we define the spray penetration as $S(t) = \sqrt{\langle z_\mathrm{p}(t)^2\rangle}$. Here, the angular brackets denote averaging over all the droplets in the cloud at a given instant of time (i.e., the parcel's instantaneous $z$ coordinate). Figure 9 depicts the spray-tip penetration into the chamber. Droplets with large $\mathrm{St_p}$ have stronger (deeper and faster) penetration, but the $\mathrm{St_p}$ dependency is still rather weak: when $\mathrm{St_p}$ increases by nearly two orders of magnitude, the penetration changes only some tens of percents. A better understanding of the data can be seen from the data in Fig. 9, in which the data in the spray penetration are plotted as a function of a dimensionless variable $\xi = (t/T)^{\eta_t}(d/D)^{\eta_d}$. As can be seen, the data collapse onto a single curve, which is nearly a straight line. We use the following parameter: $\eta_t \approx 0.65 \pm 0.05$ and $\eta_d \approx 0.15 \pm 0.03$, which corresponds to the range for which all the data collapse nearly onto a single line. It is interesting to note that in comparison to other theo-

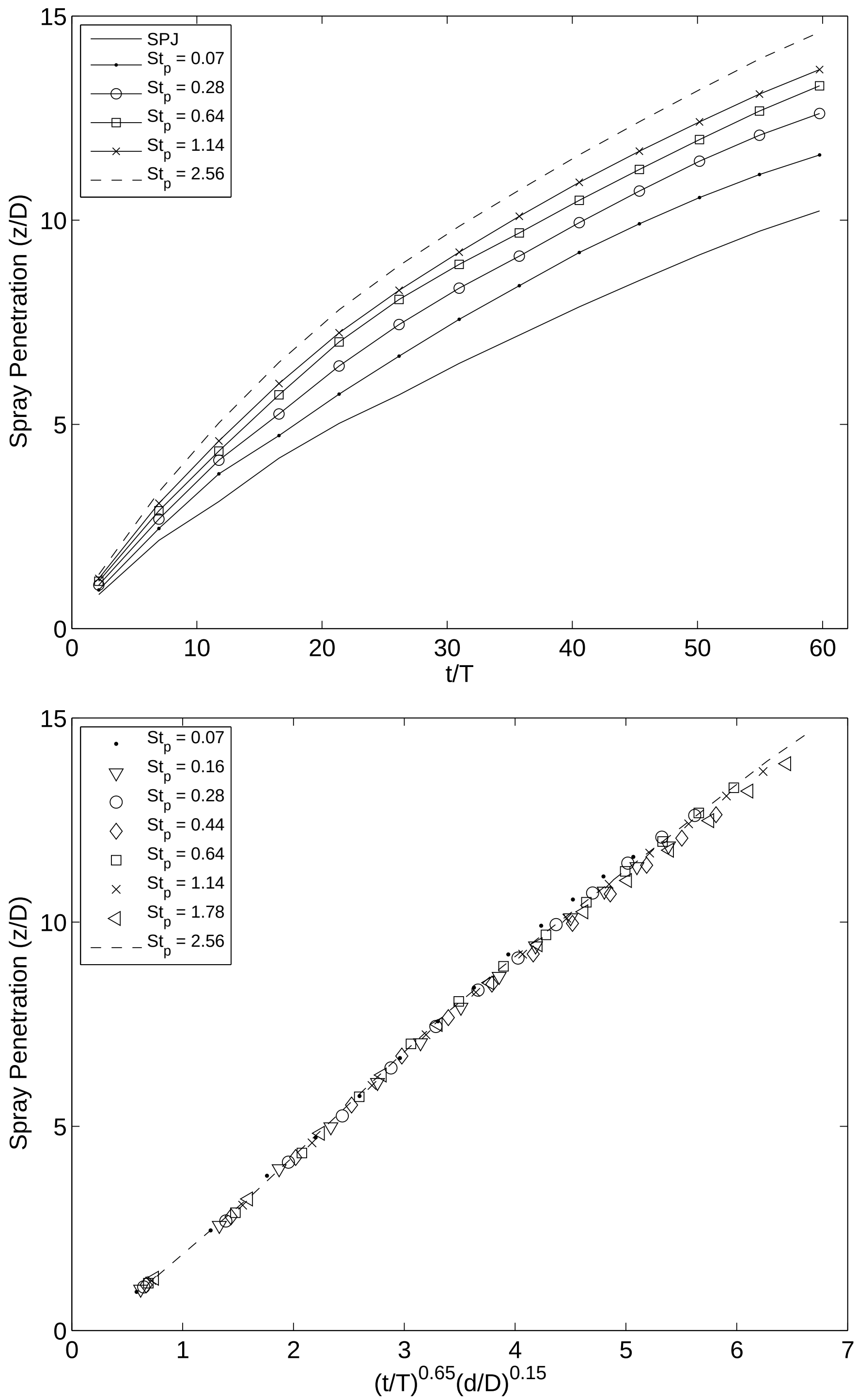


**FIG. 9:** Spray penetration defined as the RMS of droplet cloud $z$ coordinate. Droplets with increasing $\mathrm{St_p}$ have a stronger penetration. The lower panel suggests that the penetration is a function of the form $S = S(t^{0.65}d^{0.15})$.

ries on, e.g., diesel spray-tip penetration (see Heywood, 1989) a slightly larger exponent $\eta_t > 0.5$ is observed here. This seems natural because the value $\eta_t = 0.5$ corresponds to fully random motion similar to the Brownian motion. Here, in contrast, a strong axial momentum stream is present, and it is expected that $\eta_t > 0.5$. In fact, there are examples in the literature where the exponent for the spray tip penetration (note the difference to the root mean square (RMS) value as studied here) may be as high as $\eta_t = 0.8$ (Hillamo et al., 2008).

In a similar way, we define the spray width as $W(t) = \sqrt{\langle r_{\rm p}(t)^2 \rangle}$. This definition is used to quantify development of the spray width in time. The parcel's instantaneous radial coordinate is given by $r_{\rm p}(t) = \sqrt{x_{\rm p}^2 + y_{\rm p}^2}$. Figure 10 shows that $W$ behaves in a nonlinear manner for the smallest values of $\mathrm{St_p}$, but after $t = 30T$, the clouds spread in a more regular manner with a monotone increase in spray width and volume. However, for the largest value of $\mathrm{St_p}$, the spray width growth involves two different regimes. The initial growth is determined highly by the inlet conditions and the Stokes number. At later time, the width of the spray is small for the larger droples because these do not tend to follow the gaseous phase. The nonmonotone behavior of the smaller droplets shows in a very interesting fashion when $\mathrm{St_p} = 0.6$ because $W$ decreases for a short period of time but then begins to increase again. This effect is possible thanks to the fact that small droplet follow the eddies of the gaseous phase. Thus, small droplets are thrown out from the central parts of the jet, but are also transported back to the central part of the jet by the same eddies. This effect is seen for a given axial distance as a nonmonotonic behavior of the spray width (Fig. 10).

### 3.4. Droplet Trajectories and Diffusion Properties

The results presented above indicate that spray behavior can be understood in terms of droplet size. To better understand the mechanism of droplet dispersion, it is instructive to look at the trajectories of selected droplet paths. The trajectories of droplets that started at time $t = 8.5T$ are shown in Fig. 11. The trajectories that started from a region $r < D/4$ are plotted with a thick line, and the droplets that started from the region $D/4 < r < D/2$ are plotted with a thin line. Out of the selected samples the drops with $\mathrm{St_p} \sim 0.1$ are the first to interact with the shear layer vortices (i.e., are transported out of

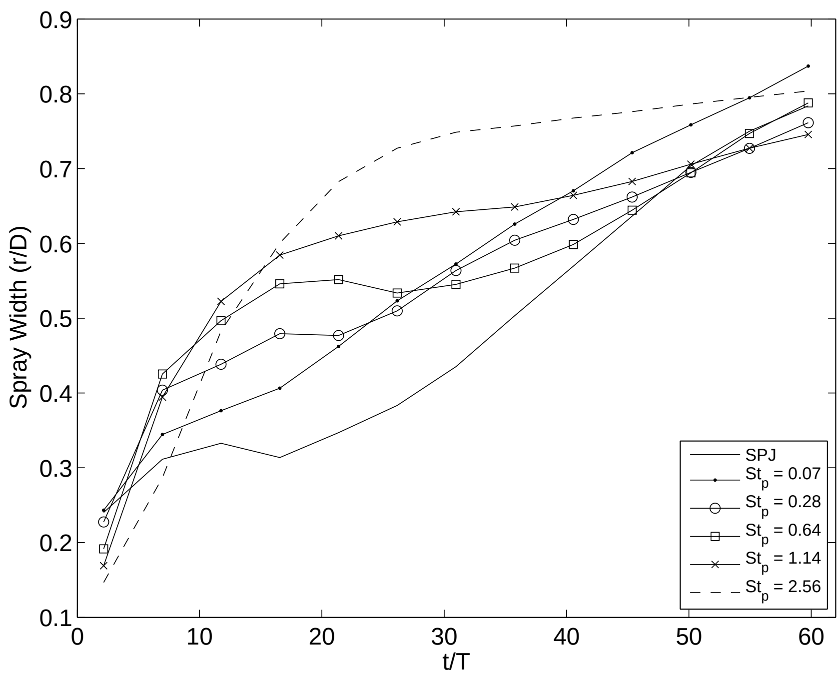


**FIG. 10:** Spray width depends strongly on $\mathrm{St_p}$.

the central region of the jet). Also, small droplets that started from the center of the jet are likely to travel rather long downstream and leave the center of the jet first after reaching the end of the potential core. As $\mathrm{St_p}$ increases, the droplet–shear-layer interaction changes nature. The role of $\mathrm{St_p}$ becomes apparent througout Figs. 11a–11d.

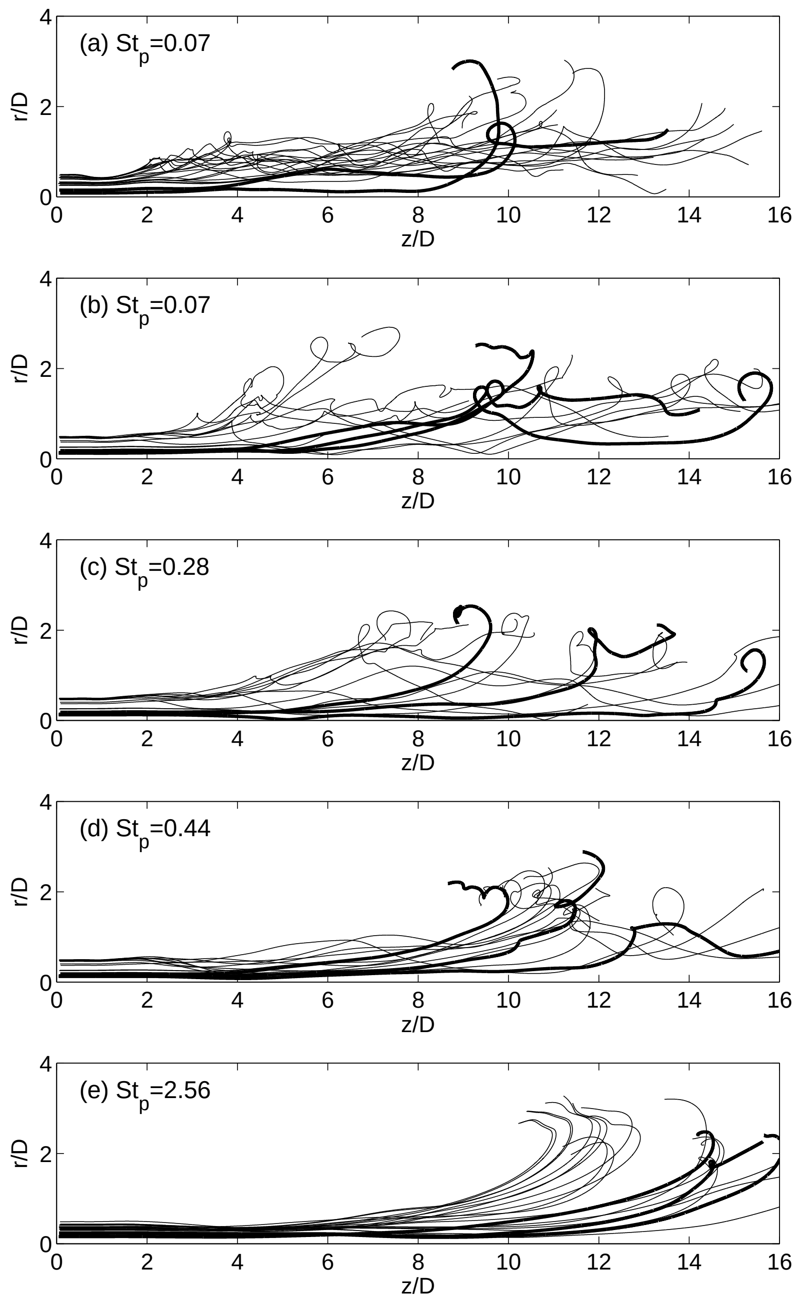


**FIG. 11:** Trajectories of the droplets that started at time $8.5T$. This figure shows that $\mathrm{St_p}$ influences the droplet-eddy interaction significantly: (a) SPJ ($\mathrm{St_p} = 0.07$), (b) PLJM ($\mathrm{St_p} = 0.07$), (c) PLJM ($\mathrm{St_p} = 0.28$), (d) PLJM ($\mathrm{St_p} = 0.43$), and (e) PLJM ($\mathrm{St_p} = 2.56$).

Especially, as can be seen from Figs. 11d and 11e, for which $\mathrm{St_p} = 0.43$ and $\mathrm{St_p} = 2.56$, respectively: the droplets are much less affected by the shear-layer vortices.

### 3.5. Droplet Probability Density Functions

The observations on differences among cloud shapes depends on the individual droplet size, its original distribution, and the droplet momentum. Further insight to the cloud shape can be gained through analysis of droplet-velocity and slip-velocity statistics. At the start of injection, the PDF of droplet velocity is ideally a $\delta$ function because all the droplets are injected with the same initial velocity $1.25U_o$. Also the slip-velocity distribution at the time $t = 0$ is a peak like function that only depends on the inlet gas-velocity fluctuation. As time goes on, more droplets are introduced into the system and the droplets are subject to the flow of the gas phase and, thereby, the droplet velocity PDF evolves in time. As new droplets are introduced to the system at a constant rate, the droplets decelerate and start to adapt to local flow conditions over a timescale $\tau_\mathrm{p}$. The droplets interact with gas-phase flow structures if the eddy turn over time is close to $\tau_\mathrm{p}$. If a finite injection time is being considered, then the time evolution of the droplet-level PDFs should have a strong role on spray cloud formation, because the droplet velocity and especially slip velocity statistics determine the strength of the interphase coupling and the momentum source term acting on the gas phase.

In the following discussion, we neglect the transient details from the early times and consider the droplet level PDFs at later times to explain differences between the developed spray shapes. All the PDFs presented have been sampled from five instants of time at intervals of $100\Delta t$ centered around the time $t = 50T$. Figure 12 shows the PDF of axial component of slip velocity. As can be seen, it is highly probable to meet large droplets in the system that have high slip velocities. A good example of this is seen in the case PLJM ($\mathrm{St_p} = 2.56$) for which the PDF shows a different behavior than the corresponding PDF for smaller $\mathrm{St_p}$. This implies that the interaction between the droplet phase and the gaseous phase last over a longer period of time and that the relaxation time of the PDF depends on $\mathrm{St_p}$. At time $t = 50T$, the PDF for which $\mathrm{St_p} < 1.5$ has nearly achieved an equilibrium-like state, but the distributions for which $\mathrm{St_p} > 1.5$ are still showing strong interaction with the axial streamwise flow. This effect can also be seen visually from Fig. 7 which implies that there are dense and dilute regions in the spray along the center region. Thus, the axial slip-velocity distributions imply that there is a strong axial velocity interaction between the large droplets and the gasous phase that lasts over much longer time than the relaxation time upon which $\mathrm{St_p}$ is based. The PDF of radial slip velocity $\delta W_\mathrm{r}$ is shown in Fig. 13. Figure 13 implies also that small droplets are likely to have smaller slip velocities than the large droplets, which do not follow the gas-phase well. The plot on a semilogarithmic scale implies that the PDF decays as $\sim \exp(-\kappa_1 \delta W_\mathrm{r})$, where $\kappa_1$ depends strongly on $\mathrm{St_p}$.

Finally, we consider the PDF of the radial component of the droplet velocity. Figure 14 depicts the radial slip velocity. The decay of the radial slip velocity is weaker as compared to the corresponding axial slip-velocity (Fig. 12). Additionally, there is a major difference between the two slip velocity components due to the initial axial momentum. Large droplets have large axial momentum and lose it slowly, whereby the changes in the slip axial velocity are smaller as compared to the corresponding radial slip velocity. The situation is opposite for the small droplets, which show larger variations in both slip-velocity components as compared to particles with large $\mathrm{St_p}$. This effect explains the slow decay of the tail of the PDF in Fig. 14 for the droplets with low $\mathrm{St_p}$. In contrast, the droplets with high $\mathrm{St_p}$ respond slowly to the radial motions, but at some point, their radial dispersion increases and they start gaining cross-streamwise momentum. Because for these droplets $\mathrm{St_p}$ is larger than unity, the adaptation time to the local flow conditions is long. As the spray spreads radially, the droplets enter into a gas with low speed in the periphery of the spray and, hence, the droplets decelerate.

Figure 15 summarizes the findings at later times as a function of $\mathrm{St_p}$: large $\mathrm{St_p}$ implies large mean slip velocity in the radial and axial components. The slip velocities in the radial component turn out to be somewhat larger than the corresponding axial components, which can be explained by initial and boundary conditions. A plot of the corresponding values for the polydisperse spray implies that these droplets follow a similar behavior. The lower panel of Fig. 15 shows that although the mean slip velocity of small droplets is small, the standard deviation may still be large. This is a sign of the dissipative nature of small droplets, which manifests itself more strongly at high mass loading ratio and has been demonstrated by Vuorinen et al. (2007).

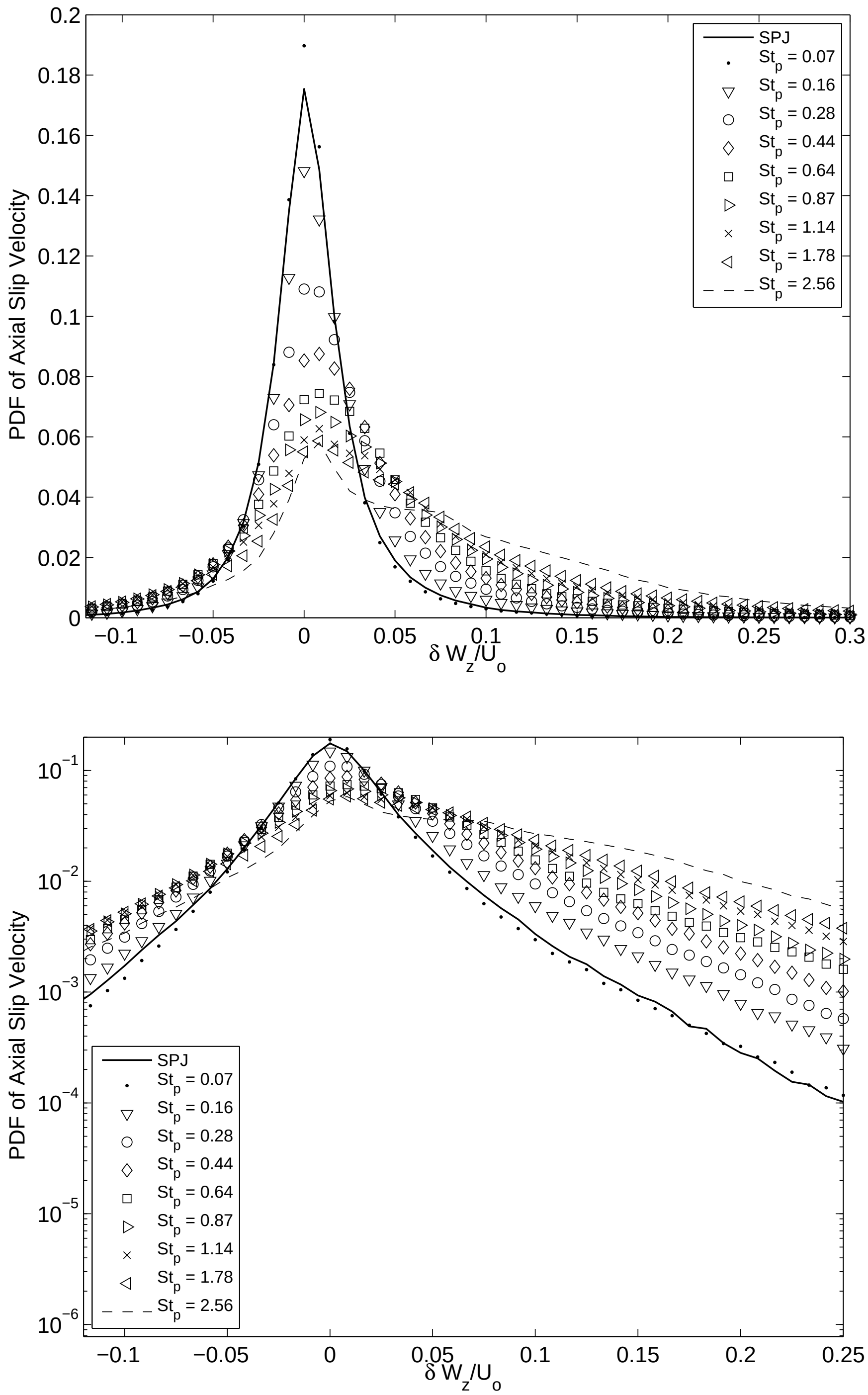


**FIG. 12:** PDF of axial slip velocity computed over the whole droplet cloud. It can be clearly seen that the PDF of the large droplets is more upward shifted than that of the small droplets. Thus, they may propagate more independently. The lower plot implies that the decay of the tails of the PDFs could be of exponential character.

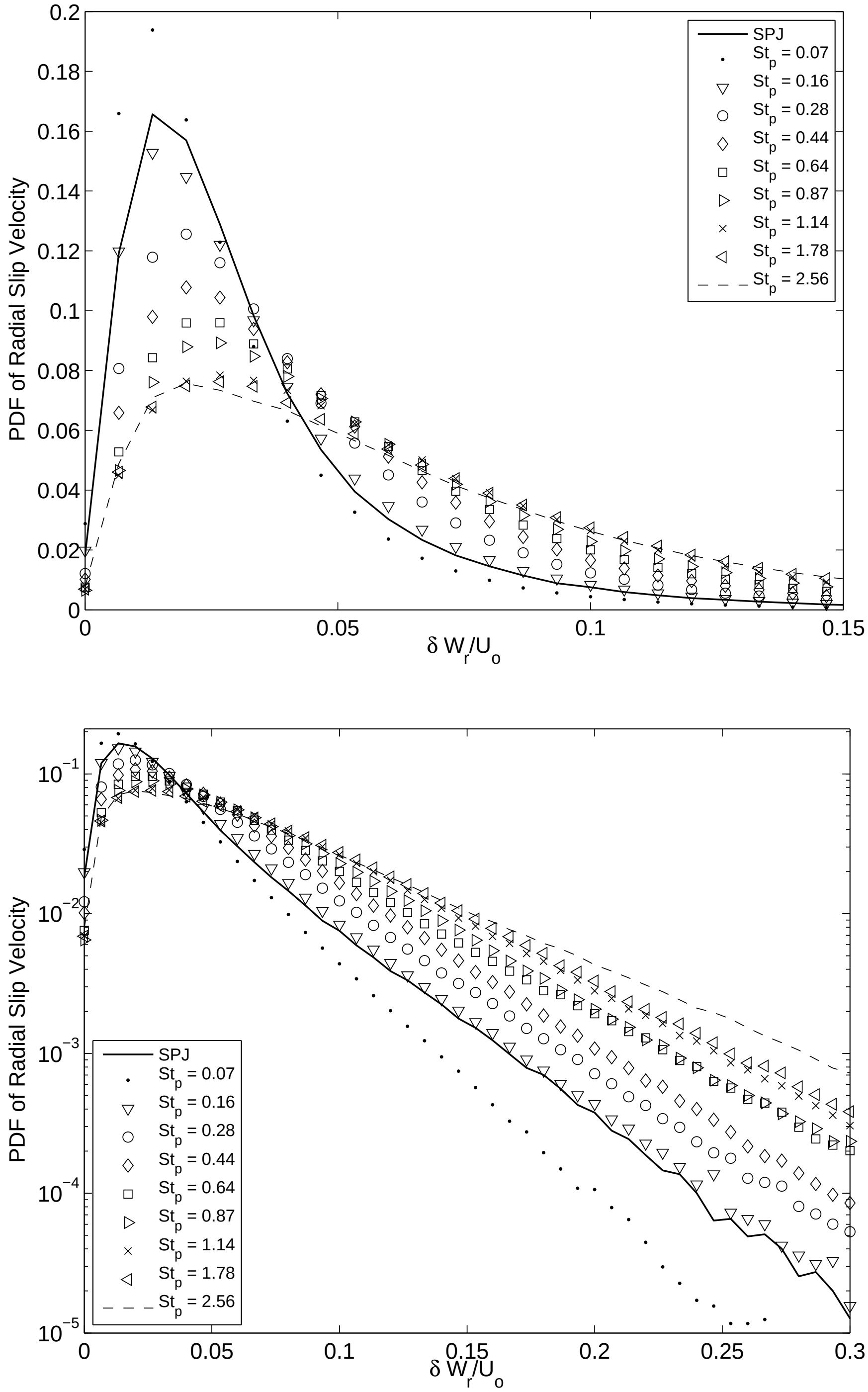


**FIG. 13:** PDF of radial slip velocity computed over the whole droplet cloud. Droplets with increasing $St_p$ may attain higher slip velocities, not only in the axial but also in the radial direction. The lower plot implies that the tails of the radial slip velocity PDF decay exponentially.

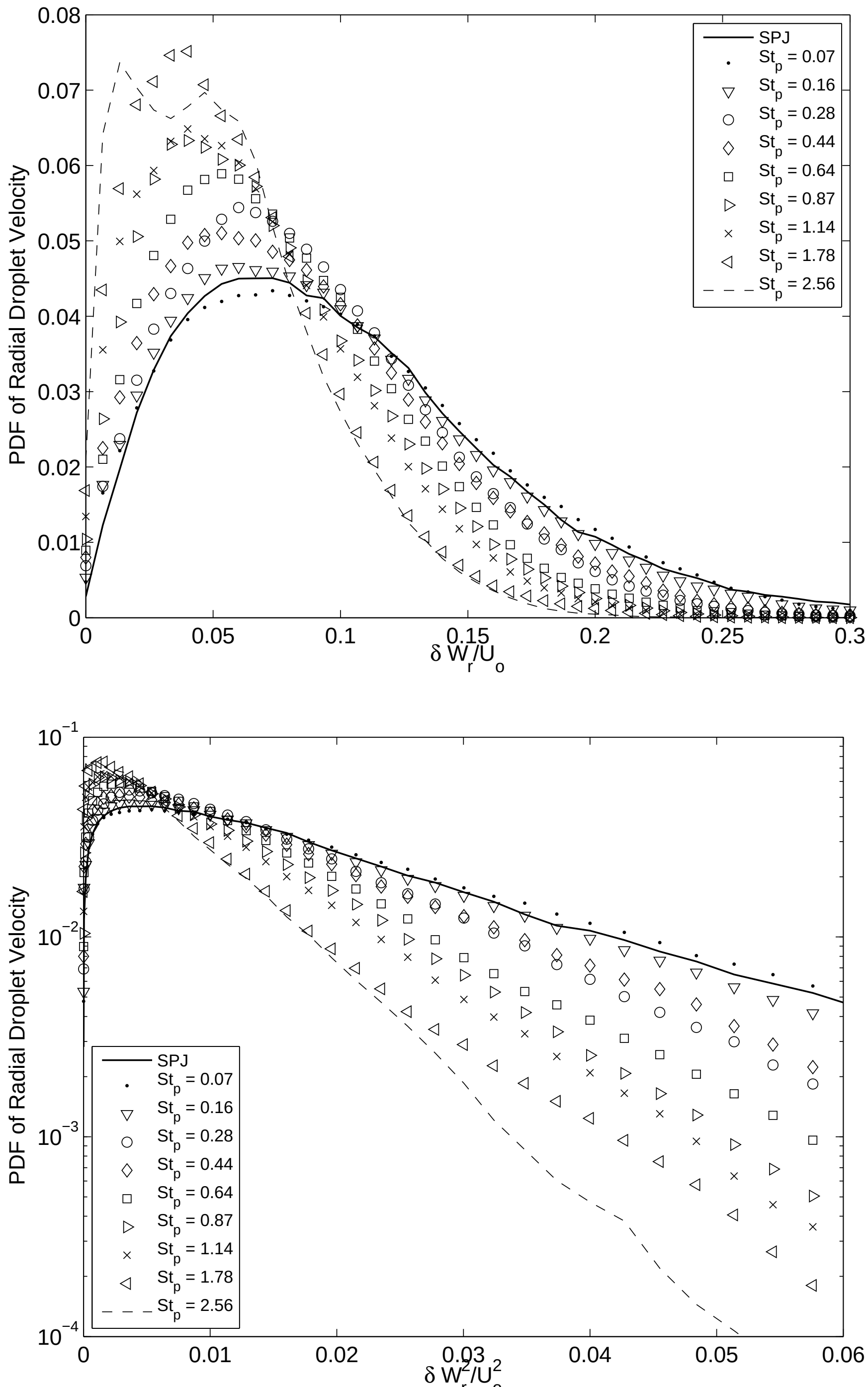


**FIG. 14:** PDF of radial droplet velocity computed over the whole droplet cloud. Small droplets are likely to attain higher radial velocities in the radial direction and hence they spread better. The lower plot indicates that the decay of the tail of the PDF of $\delta W_r^2$ is of exponential character.

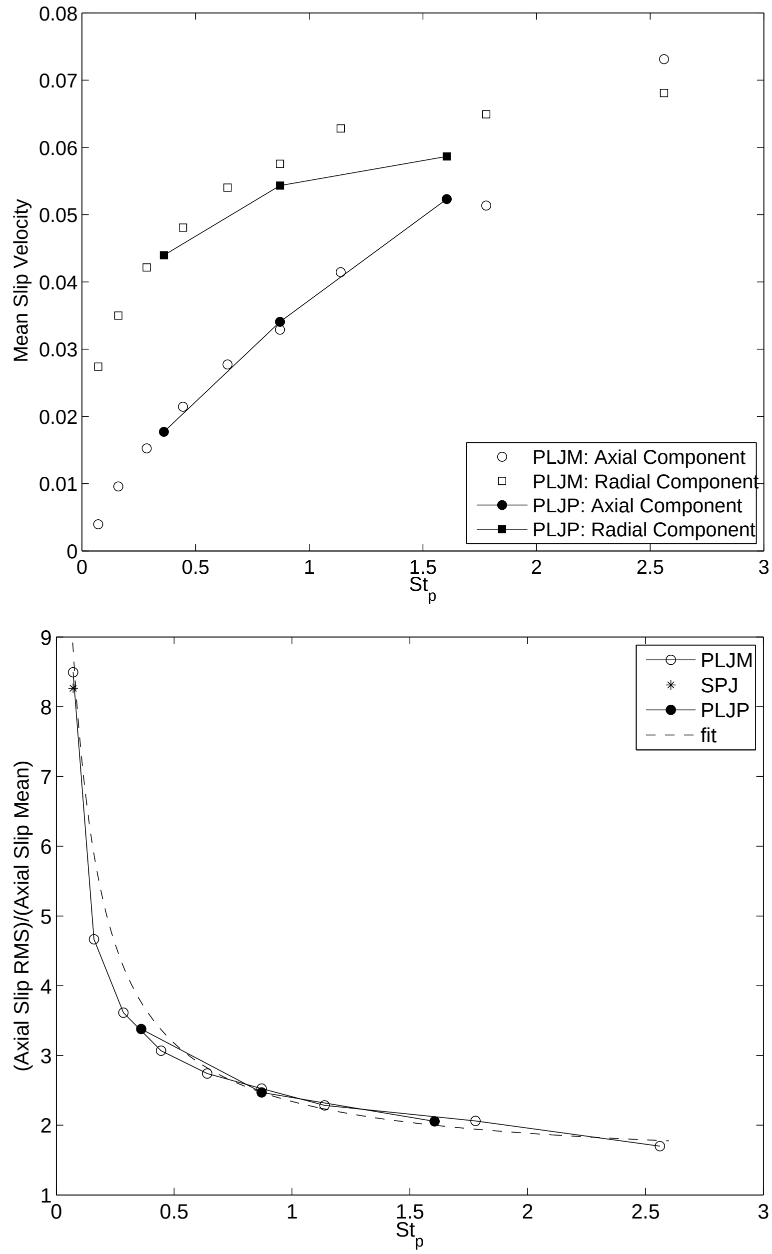


**FIG. 15:** Top: Mean axial particle velocity. Increasing $St_p$ implies larger average slip velocity. Bottom: Ratio of RMS and mean velocities for the mono- and polydisperse jet (PLJM and PLJP) cases and SPJ. In the prevailing turbulence conditions, small droplets are efficiently mixed in the turbulence due to low slip velocities.

## 4. CONCLUSIONS

The formation of spray clouds in a droplet-laden turbulent jet has been studied with the goal of enriching the picture of transient features of the Stokes number effects to the spreading of the spray. The results are of advantage in future LES and DNS studies of IC-engine sprays, where the spray dispersion needs to be properly accounted for. The cloud shapes are characteristic to the present applications and qualitatively match (1) the description on spray shapes found in the literature and (2) random characteristics of experimental diesel sprays. It was shown that the presented PLJ emulates the real diesel fuel spray shape surprisingly closely, and a lot of useful information can be extracted of droplet size effects using LES+LPT. The main observation in the paper is that the droplets couple to the flow field via the slip velocity in the momentum equation. Hence, the spray behavior may be very coherently explained through the instantaneous slip-velocity statistics. The findings of the paper may be summarized as follows:

1. A new spray penetration correlation law has been suggested. The relation implies that spray penetration for the studied mass loading can be predicted by two variables (i.e., the droplet diameter and the elapsed time according the following relation variable $\xi = t^{0.65\pm0.05} d^{0.15\pm0.03}$). However, the width of the spray is shown to behave in somewhat more complex way and cannot be expressed in a similar simple relation.

2. The droplet trajectories were visualized for various Stokes numbers. This analysis proved to be revealing from the viewpoint of turbulent mixing of droplets. The analysis revealed explicitly that the Stokes number could be used as an indicator for the size scale of the eddies with which the droplet are likely to interact: small droplets are able to interact with the small eddies but the large droplets interact mostly with the more energetic flow structures. The visualization showed that the large droplets exit the center of the jet much later than the small droplets, which is an implication that they are not efficiently mixed in the turbulence at early times. However, the lateral dispersion of the large droplets was noted to be enhanced later downstream as the size of the shear-layer vortices increase in size.

3. The shape of the clouds has been explained by analyzing the PDF of instantaneous/short-time-averaged droplet statistics. The results show that the cloud formation can be understood by considering the global PDF of axial and radial components of droplets velocity and slip velocity. Droplets with a small Stokes number have typically a small slip velocity and thereby follow the gas-phase flow better. Thus, turbulent fluctuations enhance the small droplet dispersion. In contrast, particles with a large Stokes number are likely to have large slip velocities and do not follow the fluctuating fluid equally well if the droplet time scale is large compared to a properly chosen fluid time scale. Subsequently, sprays with small droplets typically form a foglike cloud whereas the spray with large droplets typically forms a cloud where particles are first concentrated in the center and apparently show some kind of interactions with the axial mode of the jet. However, the radial spreading of the large droplets is enhanced downstream, outside the potential core region. We note that, in general, the transient analysis of droplet velocity and slip velocity PDF may serve as an interesting multiphase flow analysis method to differentiate between different particle sizes and time evolution of particle clouds in computational and experimental studies.

The given discussion implies that the results presented herein are adequate. Yet, it is clear that the simulation of dense sprays using LES/DNS+LPT remains a problem. When the local spray volume fraction increases, one option is to take this aspect into account in the spray momentum equations (Kärrholm, 2008). However, as the grid spacing decreases the point-particle assumption becomes invalid. In the case of small droplets ($\mathrm{St_p} \ll 1$) using a continuum approach for the droplet concentration [$n = n(x, y, z, t)$] could be possible and save lots of computational efforts. Regarding nearly all CFD-codes, specifically when doing LES/DNS + LPT, a problem is the parcel approach because the number of parcels has to increase when the grid spacing decreases. If the problem is approached only from the viewpoint of numerical stability of a CFD solver, then one option is to share the parcel-originated momentum among several cells, which avoids the unphysically large momentum release/absorption locally. However, despite the difficulties, because DNS of droplet-laden flows is still rather limited to very small scale applications (Lebas et al., 2009), LES+LPT are likely to prevail for decades as useful research tools.

## ACKNOWLEDGMENTS

The financial help from the Finnish Graduate School of Energy Technology and the Finnish Technology Foundation is deeply acknowledged. The authors also thank CSC—IT Center for Science Ltd. for providing the support regarding installation of OpenFOAM on supercomputing environment and computational resources for this study.

## REFERENCES

Akihama, K., Takatori, Y., Inagaki, K., Sasaki, S., and Dean, A. M., *Mechanism of the smokeless rich diesel combustion by reducing temperature*, SAE Technical Paper Series 2001-01-0655, 2001.

Amsden, A. A., O'Rourke, P. J., and Butler, T. D., KIVA-II: A computer program for chemically reactive flows with sprays, Technical Report No. LA-11560-MS, Los Alamos National Laboratory, 1989.

Apte, S., Mahesh, K., Moin, P., and Oefelein, J. C., Large-eddy simulation of swirling particle-laden flows in a coaxial-jet combustor, *Int. J. Multiphase Flow*, vol. 29, pp. 1311–1331, 2003a.

Apte, S., Gorokhovski, M., and Moin, P., LES of atomizing spray with stochastic modeling of secondary breakup, *Int. J. Multiphase Flow*, vol. 29, pp. 1503–1522, 2003b.

Apte, S., Mahesh, K., and Moin, P., Large-eddy simulation of evaporating spray in a coaxial-jet combustor, *Proc. of the Combustion Institute*, vol. 32, pp. 2247–2256, 2009.

Berglund, M., Large-eddy simulation of complex turbulent flows, PhD Thesis, Lund, Sweden, 2006.

Borman, G. K. and Ragland, K. W., *Combustion Engineering*, McGraw-Hill, New York, 1998.

Cao, Z., Nishino, K., Mizuno, S., and Torii, K., PIV measurement of internal structure of diesel fuel spray, *Exp. Fluids*, vol. 29, pp. S211–S229, 2000.

Crowe, C. T., Sommerfeld, M., and Tsuji, Y., *Multiphase Flows with Droplets and Particles*, CRC Press, Boca Raton, 1998.

Eaton, J. and Fessler, J., Preferential concentration of particles by turbulence, *Int. J. Multiphase Flow*, vol. 20, pp. 169–209, 1994.

Elghobashi, S., On predicting particle-laden turbulent flows, *Appl. Sci. Res.*, vol. 48, pp. 301–314, 1991.

Elghobashi, S., Particle-laden turbulent flows: Direct simulation and closure models, *Appl. Sci. Res.*, vol. 52, pp. 309–329, 1994.

Ferrand, V., Bazile, R., Borée, J., and Charnay, G., Gas-droplet turbulent velocity correlations and two-phase interaction in an axisymmetric jet laden with partly responsive droplets, *Int. J. Multiphase Flow*, vol. 29, pp. 195–217, 2003.

Ferziger, J. and Perić, M., *Computational Methods for Fluid Dynamics*, Springer-Verlag, Berlin, 1999.

Grinstein, F. F., Fureby, C., and DeVore, C. R., On MILES based on flux-limiting algorithms, *Int. J. Numer. Methods Fluids*, vol. 47, pp. 1043–1051, 2005.

Grinstein, F. F. and Fureby, C., Recent progress on flux-limiting based implicit large eddy simulation, European Conference on Computational Fluid Dynamics, ECCOMAS CFD, 2006.

Grinstein, F. F., Margolin, L. G., and Rider, W. J., *Implicit Large Eddy Simulation*, Cambridge University Press, Cambridge, England, 2007.

Hällqvist, T., Large eddy simulation of impinging jets with heat transfer, PhD Thesis, KTH, Stockholm, 2006.

Heywood, J., *Internal Combustion Engine Fundamentals*, McGraw-Hill, New York, 1989.

Hillamo, H., Kaario, O., and Larmi, M., PIV measurements of a diesel spray, SAE Paper No. 2008-08PFL-552, 2008.

Hori, T., Senda, J., Kuge, T., and Fujimoto, H., Large eddy simulation of non-evaporative and evaporative diesel spray in constant volume vessel by use of KIVALES, SAE Paper No. 2006-01-3334, 2006.

http://www.opencfd.co.uk/, 2010.

Jasak, H., Error analysis and estimation for the finite volume method with applications to fluid flows, PhD Thesis, Imperial College, London, 1996.

Kärrholm, F. P., Numerical modelling of diesel spray injection, turbulence interaction and combustion, PhD Thesis, Chalmers University of Technology, Göteborg, 2008.

Kärrholm, F. O. and Nordin, N., Three-dimensional simulation of diesel spray ignition and flame lift-off using OpenFOAM and KIVA-3V CFD codes, SAE Technical Paper Series 2008-01-0961, 2008.

Kenning, V. M. and Crowe, C. T., On the effect of particles on carrier phase turbulence in gas-particle flows, *Int. J. Multiphase Flow*, vol. 23, pp. 403–408, 1997.

Lebas, R., Menard, T., Beau, P. A., Berlemont, A., and Demoulin, F. X., Numerical simulation of primary break-up and atomization: DNS and modeling study, *Int. J. Multiphase Flow*, vol. 35, pp. 247–260, 2009.

Lieuwen, T. and Yang, V., *Combustion Instabilities in Gas Turbine Engines: Operational Experience, Fundamental Mechanisms and Modeling*, Progress in Astronautics and Aeronautics, vol. 210, AIAA, USA, 2005.

Ling, W., Chung, J., Troutt, T., and Crowe, C., Direct numerical simulation of a three dimensional temporal mixing layer with particle dispersion, *J. Fluid Mech.*, vol. 358, pp. 61–85, 1998.

Longmire, E. K. and Eaton, J., Structure of a particle-laden round jet, *J. Fluid Mech.*, vol. 236, pp. 217–257, 1992.

Luo, K., Klein, M., Fan, J.-R., and Cen, K., Effects on particle dispersion by turbulent transition in a jet, *Phys. Lett. A*, vol. 37, pp. 345–350, 2006.

Naber, J. D. and Siebers, D. L., Effects of gas density and vaporization on penetration and dispersion of diesel sprays, SAE Technical Paper Series 1996-960034, 1996.

Oefelein, J. C., Sankaran, V., and Drozda, T. G., Large eddy simulation of swirling particle-laden flows in a model axisymmetric combustor, *Proc. of Combustion Institute*, vol.

31, pp. 2291–2299, 2007.

Olsson, M. and Fuchs, L., Large eddy simulation of the proximal region of a spatially developing circular jet, *Phys. Fluids*, vol. 8, pp. 2125–2137, 1996.

Pickett, L. M. and Siebers, D. L., Orifice diameter effects on diesel fuel jet flame structure, *J. Eng. Gas Turbines Power*, vol. 127, pp. 187–196, 2005.

Pope, S., *Turbulent Flows*, Cambridge University Press, Cambridge England, 2001.

Salewski, M. and Fuchs, L., Consistency issues of lagrangian particle tracking applied to a spray jet in crossflow, *Int. J. Multiphase Flow*, vol. 33, pp. 394–410, 2007.

Siebers, S. and Higgins, B., Flame lift-off on direct-injection diesel sprays under quiescent conditions, SAE Technical Paper Series 2001-01-0530, 2001.

Stiesch, G., *Modeling Engine Spray and Combustion Processes*, Springer-Verlag, Berlin, 2003.

Vuorinen, V., Larmi, M., and Fuchs, L., Large-eddy simulation of spray-originated turbulence production and dissipation, S4_Tue_A_14, *Proceedings of 6th Int. Conference on Multiphase Flow, ICMF-2007*, Leipzig, 2007.

Vuorinen, V., Larmi, M., and Fuchs, L., Large-eddy simulation of particle size distribution effects on turbulence in sprays, *Proceedings of 45th AIAA Aerospace Sciences Meeting and Exhibit*, Grand Sierra Resort, Reno, AIAA Paper No. AIAA-2008-0514, 2008.

Yan, J., Luo, K., Fan, J., Tsuji, Y., and Cen, K., Direct numerical simulation of particle dispersion in a turbulent jet considering inter-particle collisions, *Int. J. Multiphase Flow*, vol. 34, pp. 723–733, 2008.